Calibrating the Non-Common Path Aberrations on the MOAO system RAVEN and first science results using RAVEN

Masen Lamb[a,b], David R. Andersen[b], Jean-Pierre Véran[b], Carlos Correia[c], Olivier Lardière[a,b]

[a]University of Victoria, 3800 Finnerty Rd, Victoria, BC, Canada;
[b]NRC Herzberg Astronomy, 5071 W. Saanich Rd, Victoria, BC, Canada; [c]Centre for Astrophysics, University of Porto, Porto, Portugal; [d]University of Manitoba, 66 Chancellors Cir, Winnipeg, MB, Canada;

ABSTRACT

Contemporary AO systems, such as the Multi-Object Adaptive Optics system (MOAO) RAVEN currently associated with the Subaru Telescope, can suffer from significant Non-Common Path Aberrations (NCPA). These errors ultimately affect image quality and arise from optical path differences between the wavefront sensor (WFS) path and the science path. A typical correction of NCPA involves estimating the aberration phase and correcting the system with an offset on the deformable mirror (DM). We summarize two methods used to correct for NCPA on an experimental bench. We also successfully calibrate the NCPA on RAVEN using one of these methods. Finally, we report on some first science results with RAVEN, obtained after NCPA correction.

Keywords: Wavefront Sensing, NCPA Calibration, Phase Diversity, Image Sharpening

1. INTRODUCTION

Optical elements in Adaptive Optics (AO) systems such as lenses and mirrors can suffer from imperfections in polishing or coating processes; therefore if these elements exist after the beamsplitter in a simple AO system (in either the WFS path or the Science path) they induce what are known as Non-Common Path Aberrations (NCPA) since one path 'sees' the aberration and the other path does not. These aberrations ultimately cause a degradation in the image quality of an AO system. In the classic AO system the only major NCPA can be characterized by relatively few optical elements, such as the optical elements marked by a '*' in Figure 1 (shown in the orange optical path). However, contemporary AO systems using more advanced techniques such as multi-object AO (MOAO, see Section 5.1) or multi-conjucate AO (MCAO) host a variety of non-common optical elements between the WFS and camera arms. In such systems the NCPA can be quite significant, as is shown on the left of Figure 2 where a simulated error is applied to the deformable mirror on an experimental bench (see Section 2 for a description of the bench) and the resulting image of a point source is significantly degraded.

To correct for these errors on an adaptive optics system they must first be quantified and then applied as an offset on the deformable mirror; telescopes such as Keck have successfully done this in the past.[1] There are a variety of different ways to determine the NCPA in an AO system, two of which will be investigated and discussed in this paper. The MOAO demonstrator RAVEN is calibrated using these NCPA correction methods.

Further author information: (Send correspondence to M.L.)
M.L.: E-mail: masen@uvic.ca, Telephone: 1 604 837 6565

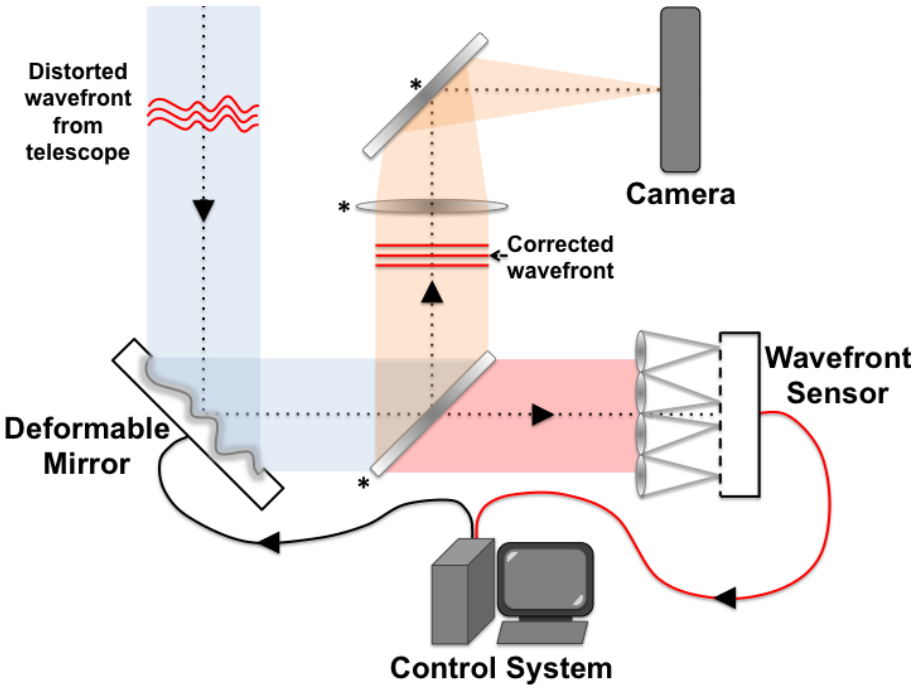

Figure 1. A classic AO system consisting of a deformable mirror (DM) and a wavefront sensor (WFS). The non-common path is shown in orange, where an optical element in this beam contributes errors not seen by the WFS (a '*' in this figure represents such an element). These errors originate from imperfections in the manufacturing of the optical elements, such as polishing or coating processes; they are known as Non-common Path Aberrations (NCPA).

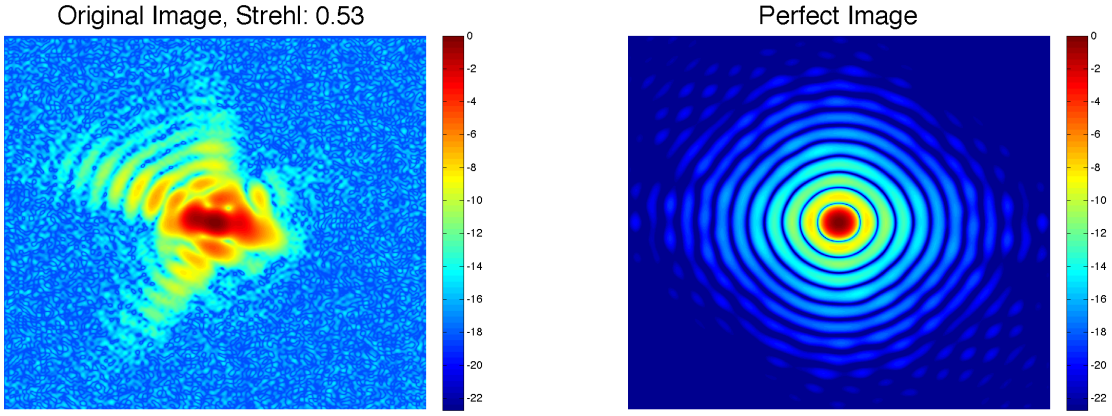

Figure 2. A log-scale image of a point source with typical NCPA polishing errors represented by a contemporary AO system (such as MOAO or MCAO), a description of how this image is created is in Section 4. When compared with a theoretical perfect PSF (right), it can be seen the image greatly suffers from NCPA aberrations if they are not compensated.

2. EXPERIMENTAL BENCH

We develop our NCPA correction methods both in simulation and on an experimental bench located at NRC-Herzberg in Victoria. The experimental bench consists of a simple AO system (see Figure 3), employing all of the necessary tools required to do this (light source, DM, WFS, computer, Cameras, etc.). We use an ALPAO DM, which consists of 97 magnetic voice-coil actuators on the surface of a 13.5 mm pupil. The WFS is a Shack-Hartmann with 3 sub apertures (lenslets) projected across each actuator on the pupil. We employ a fibre source operating at 655 nm. The PSF is well oversampled with approximately 8 pixels across the FWHM. Closing the loop on this simple AO system was straightforward and the resulting PSF was very near to perfect (shown in Figure 3), showing our system is well aligned.

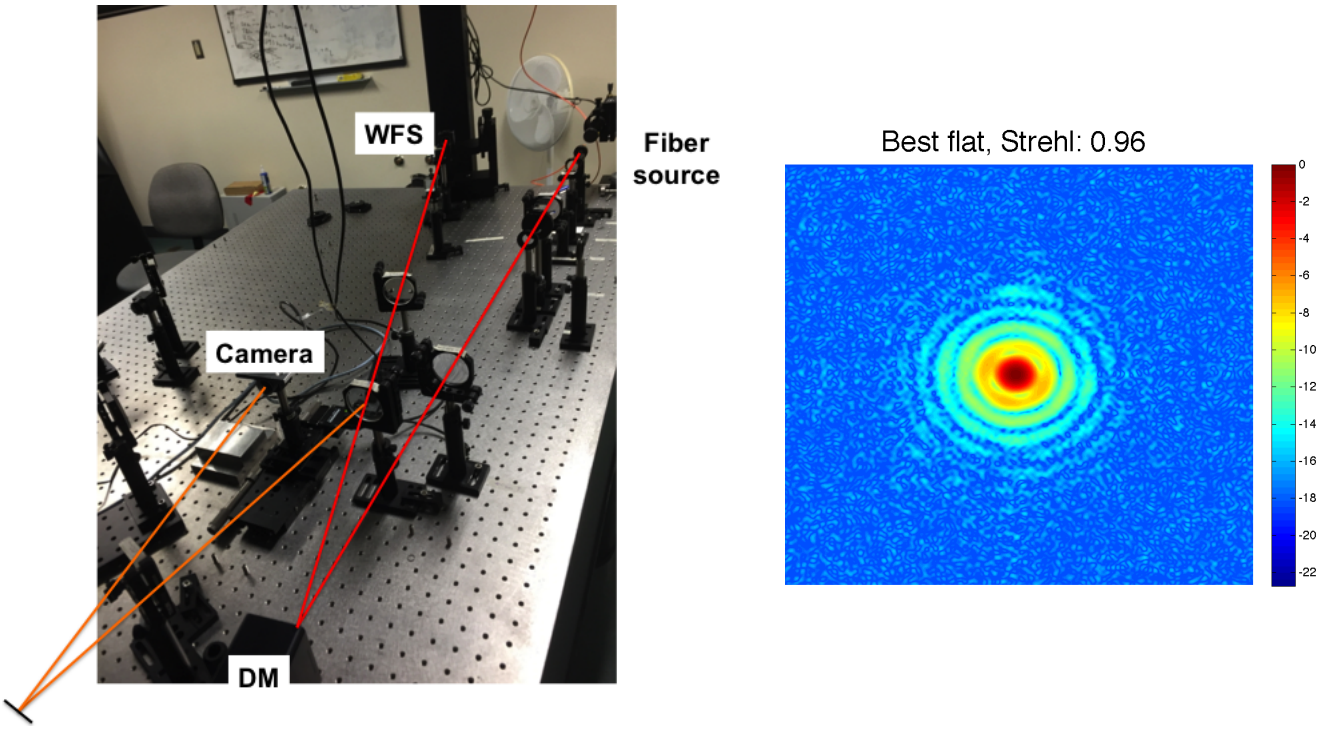

Figure 3. Left: our experimental bench at NRC-Herzberg. The orange line denotes the non-common path between the science camera and the WFS. Right: the best flat (log scale) after closing our AO loop; it can be seen our system is quite well aligned given the high Strehl ratio.

2.1 NCPA corrections using the WFS reference slopes

There are many ways to apply a desired shape to the deformable mirror, such as projecting a phase map onto the DM using the DM's influence functions. Another way to create a desired shape is to close the AO loop on a WFS spot pattern that represents the NCPA (as opposed to the traditional uniform reference grid). The benefit of this is that the desired shape is guaranteed to be created, being that the WFS will ultimately 'read' the desired shape. Furthermore, the particular DM we use can suffer from 'drift' where it can change shape over time, therefore if we use the influence functions to create our NCPA correction they may suffer from this effect. Since the AO loop is closed on these reference slopes, the system is forced to continuously take the desired shape - regardless of drift. For these reasons we adopt the reference slope method to correct our NCPA.

2.2 Stehl ratio calculations

It is important to quantify how well the calibration methods are performing, the standard metric is the Strehl ratio. There are many different ways people calculate this value, with each method yielding different results. It is therefore important to accurately describe the method we use here, which we believe to be the most commonly

accepted method.[2] We calculate the Strehl by comparing our peak intensity directly with the theoretical image (other groups use different methods) and therefore the theoretical PSF must be described as accurately as possible. The theoretical PSF is based on two main values: the plate scale and the pupil function. We first determine the pupil function by integrating each sub aperture on our WFS lenslet array, and then we determine our plate scale from initially using the bench parameters (i.e. f-number, wavelength, etc.). The plate scale rarely corresponds exactly to the theoretical bench parameters, therefore it is fine-tuned by adjusting the scale such that the residual between itself and the best measured PSF is minimized. The theoretical and measured PSF are first normalized to their peak intensity, then the measured PSF is multiplied by the ratio between the sum of the theoretical image and sum of the measured image. This ensures the images are on equal scales. The size of the image used is very important and is determined by the curve of growth, in particular where the curve begins to 'plateau'; the curve of growth is simply the total summed intensity as a function of radius from the centre of the PSF. Choosing an image size that differs by as little as 10 pixels can effect the Strehl by up to 5%, therefore the choice of this number is crucial.

3. CORRECTION TECHNIQUES

3.1 Focal Plane Sharpening

One method of quantifying the NCPA of a system is to search over different DM shapes for the set of commands that yield an optimized PSF. This can be done accurately when an optimization algorithm is employed, and efficiently if the algorithm is fast. We do this by employing a downhill simplex (aka Nelder-Mead) optimization algorithm[3] to search over an orthogonal basis that represents the phase of our DM. This algorithm uses functional evaluations and therefore is much faster than algorithms that compute, for example, analytical gradients. Furthermore, the optimization criterion of this algorithm is the peak intensity of the PSF, allowing for a very fast convergence. We call the choice of algorithm and optimization criteria *Focal Plane Sharpening* (FPS). One drawback to our selection of optimization algorithm is the potential of convergence on a local maximimum (when searching for the peak of the PSF), however if used correctly this drawback can be overcome as we will discuss later in this paper (see Section 4). Another disadvantage of this method is the requirement of many images, as each iteration requires at minimum one new image, which can be computationally cumbersome. Figure 4 summarizes the method with a block diagram.

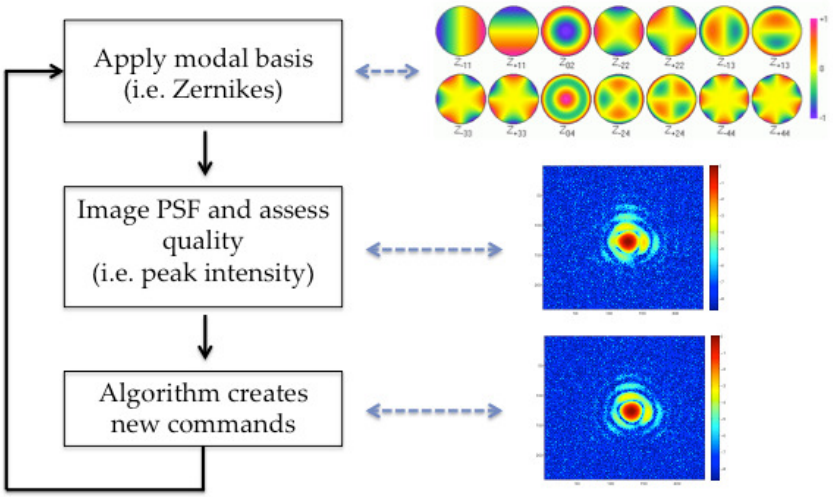

Figure 4. The method of focal plane sharpening (FPS).

3.1.1 Simulation and Experiment

Focal Plane Sharpening was explored in simulation to find an ideal basis and set of optimization parameters that could later be used on an experimental bench, the results are described in Lamb et al. (2014).[4] We simulate

NCPA by dividing a set of random Zernike coefficients by their respective radial order to approximate a $1/\nu^2$ Power Spectral Density profile, which approximates typical polishing errors (following [5]). A typical NCPA phase map profile can be seen in the top left of Figure 9. The steps for finding the NCPA are as follows:

- Start with initial DM shape (and corresponding PSF)
- Start optimization algorithm, choosing an orthogonal basis (i.e. Zernike modes), which can be applied to our DM
- Have the algorithm search over the given parameter space (i.e. all modes), sampling new basis combinations (and thus DM shapes) at each iteration
- Take images and measure the PSF at each iteration; have the algorithm assess the convergence criterion (i.e. find the peak of the PSF, minimize the FWHM of the PSF, etc.) and eventually converge

The simulations of FPS were successful (see [4]) and the method was applied on our experimental bench using a Zernike basis. One added feature in our experiment that was not included in simulation is that there are boundary conditions imposed on the Zernike coefficients. These boundary conditions follow a 1/(radial order) power law (the power law approximating NCPA) to help minimize the chance the solution will find a local minimum as well as help the speed the convergence. The Zernike shapes are created using the influence functions of the DM instead of using the reference slopes (i.e. like discussed in Section 2.1) simply because the loop would take a long time to converge. We first close the AO loop using the WFS, and then use FPS to estimate the first 21 Zernike modes to estimate NCPA correction on our simple system. We note that we do not expect much of a correction considering our system is initially near-perfect, as shown in Figure 3. FPS convergence occurs in about 1 minute and the results are shown in Figure 5: there is a Strehl increase of about 3%. Also worthy of note is the odd 'pentagon' like structure affecting the outside rings; this is due to the DM 'drifting' back to the one of its previous shapes and has absolutely nothing to do with the method of FPS. To resolve this we propose two methods for the future: either run FPS in close loop (that is use WFS reference slopes to create the DM shape as opposed to influence functions) or try to fix this DM 'drift' or 'creep'. The latter has been achieved by a group of researchers at Durham University and they have kindly shared their correction method. In the near future we will try FPS with both of these fixes.

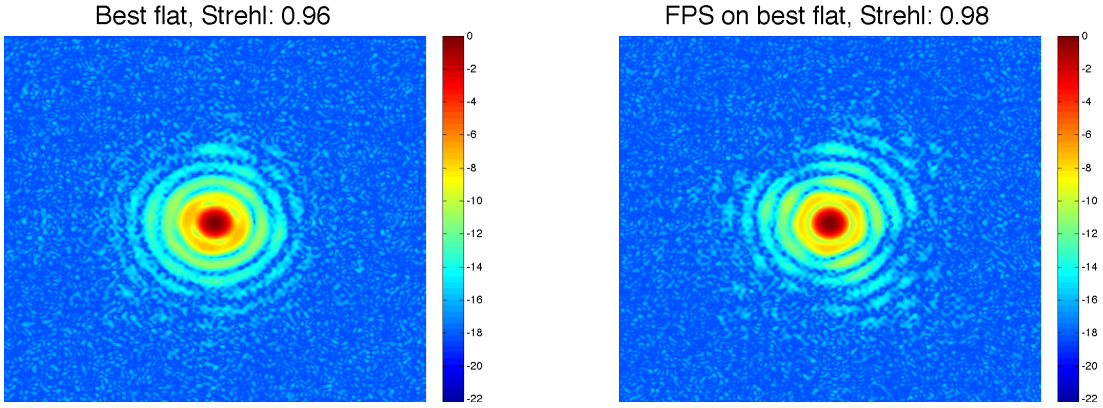

Figure 5. Focal plane sharpening applied *after* closing the AO loop (using our WFS), the AO flat is shown left while the FPS corrected image is shown right. The Strehl ratio increases, as expected if it corrected NCPA of the system. The gap between the centre and the first diffraction ring is also 'carved' out, as desired. Also worthy of note is the 'pentagon' like structure in the FPS corrected image, this is discussed in the text.

It is worth noting that throughout this bench's history, we have employed 4 different DMs, all varying in actuator number and type and this method works very well with every one of them.

3.2 Phase Diversity

The method of Phase Diversity (PD) has been employed in the past to compensate AO systems for NCPA;[1,6,7] its method relies on using images in focus and with known aberration injections (the diversity) to estimate the NCPA of the system, and is well described in the literature.[8–11] Figure 6 shows a diagram of the method. Traditionally the diversity is in the form of focus, which can be injected several different ways; for example: moving a camera on a translational stage, using two cameras (one in and on out-of focus), or applying focus directly to the DM will all cause an injected focus to the image. Carlos Correia (at Laboratoire d'Astrophysique de Marseille) has developed a code in Matlab which employs the method of Phase Diversity;[12] we explored this code in both simulation and on an experimental bench. Our simulation results are summarized in [4] and we discuss our experimental results here.

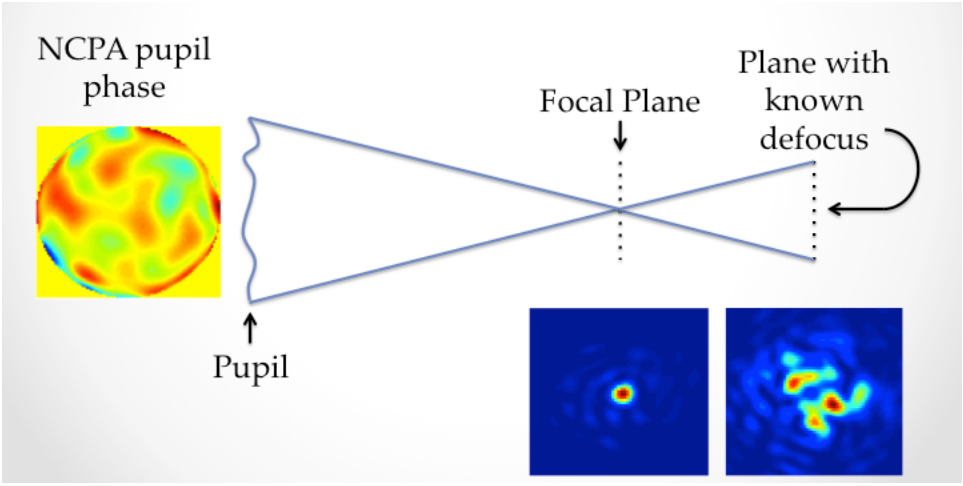

Figure 6. The method of Phase Diversity (PD).

Phase Diversity was successfully implemented on our experimental bench by exchanging the theoretical images created in simulation with real images. The parameters of the experimental bench such as pupil shape, pupil size, pupil variation, plate scale, and wavelength needed to be very accurately described before the PD algorithm would successfully converge. Extreme emphasis needs to be place on the latter point, where many countless hours were committed to accurately determining these parameters. The code has the ability to use several images (one in focus and N aberrated images) to estimate the phase of the system. Through experimentation, we found the best number of images were 7 in total: 3 on other side of the focus (at anti-symmetric positions, spanning from -1.5 to 1 wave) and 1 in focus (see Figure 7). In general, increasing the number of images both increases accuracy and reduces the computational time of the NCPA estimation. Furthermore, if there was an increase in a bench parameters uncertainty (i.e. the size of the pupil, etc.), the code would perform better if more images were used. As a check to ensure the code was working correctly, Zernike modes astigmatism and coma were purposely injected to the system and then successfully recovered with the Phase Diversity estimation. We chose to estimate the first 21 Zernike modes using Phase Diversity; this number of modes was chosen arbitrarily, as the main goal of this work is to compare this method with Focal Plane Sharpening and the number of estimated modes is not overly important. The results are shown in Figure 8.

4. EXPERIMENTAL RESULTS

As shown in the previous section, both Focal Plane Sharpening and Phase diversity can compensate the NCPA on an already near-perfect AO system, with Focal Plane Sharpening slightly outperforming Phase Diversity. At first glance, this suggests the former method might be more desirable than the latter. We now aim to quantify how each method performs when dealing with more complex AO systems that suffer from significantly more NCPA than what exists on our current bench. We simulate more complex AO systems by simply creating a phase map representative of the NCPA of such an AO system, and then closing the AO loop on the reference

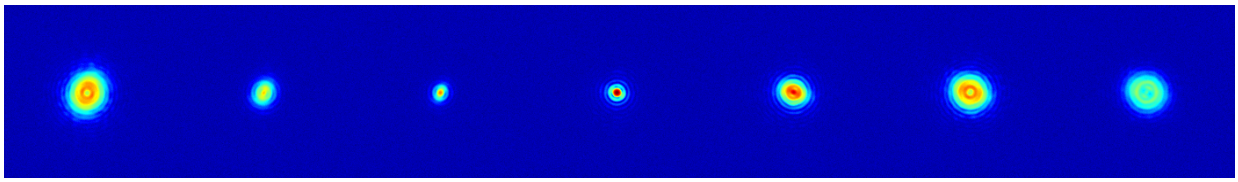

Figure 7. The seven images used in our Phase Diversity experiment. The images are taken over the range from -1.5 waves to +1.0 waves, at uneven increments (with the middle image corresponding to 'in-focus'.)

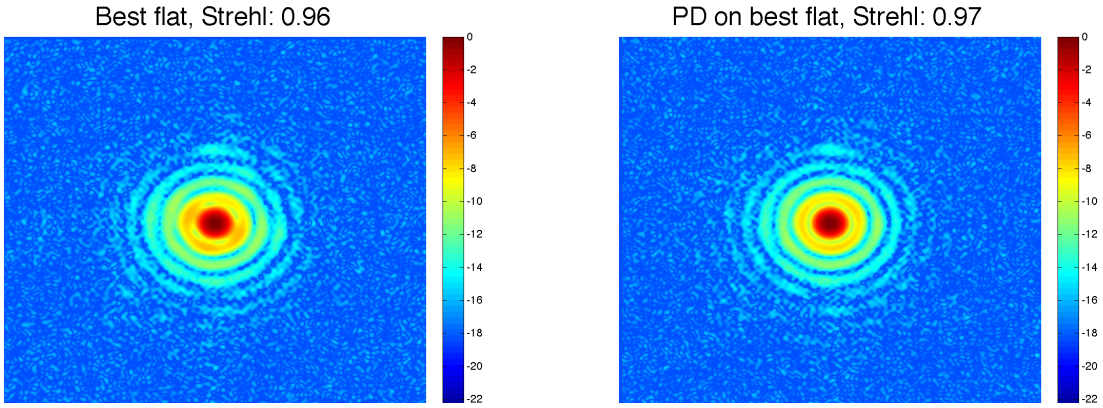

Figure 8. Left: best flat from closing the AO loop on our WFS. Right: Phase Diversity correction on the initial AO flat. Note, the Strehl improvement is *not* as much as the FPS improvement on the same initial image.

slopes pertaining to this phase. The phase map is created by using a random vector (between -1 and 1) of 21 Zernike mode coefficients, and dividing each mode by its radial order. This phase map is normalized to 75 nm RMS wavefront error, it is shown in Figure 9. A theoretical vector of WFS slopes is created from this phase map and the AO loop is closed on these reference slopes, thereby creating the PSF shown in Figure 9.

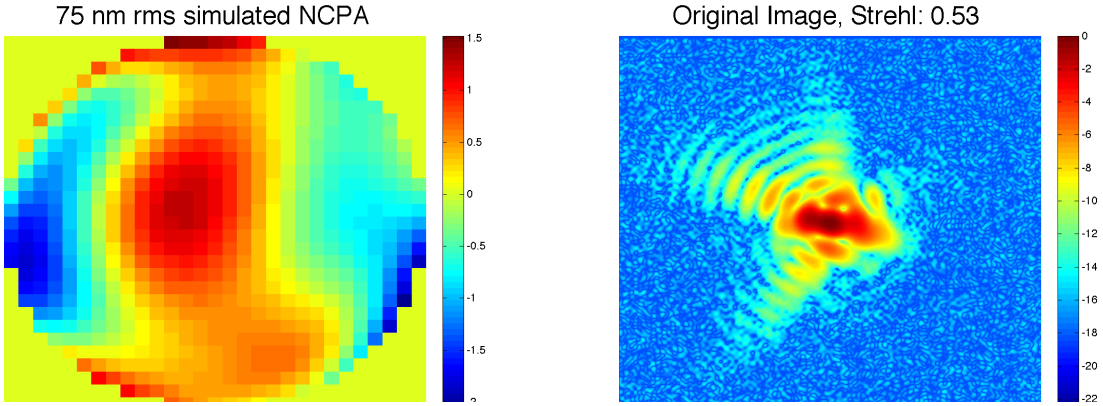

Figure 9. Left: NCPA phase map corresponding to typical polishing errors at a strength of 75 nm rms. The shape was created by closing the loop on the reference slopes that pertain to this phase map. The resulting PSF shape is shown on the right.

The two methods were applied to this error-injected PSF and their corrected images are shown in Figure 10. It appears that Phase Diversity has recovered the original phase as the Strehl of this image is identical to the Phase Diversity correction if there is *no* injected-error. Conversely, it appears FPS gets stuck in a local maximum, given the general shape of the image, however it is still worthy to note the Strehl is improvement is

still quite high. To assess weather the method of Phase Diversity completely recovered the initial phase we plot the estimated Zernike polynomials with the actual known NCPA Zernikes that were injected into the system. This is shown in Figure 11 (right), where it is obvious the estimated Zernikes almost completely overlap with the injected Zernikes. Another assessment of Phase Diversity was to see if performing multiple iterations improved our NCPA correction results. The result is shown in Figure 11, where the results from another iteration of Phase Diversity (using the previous PD corrected images as a starting point).

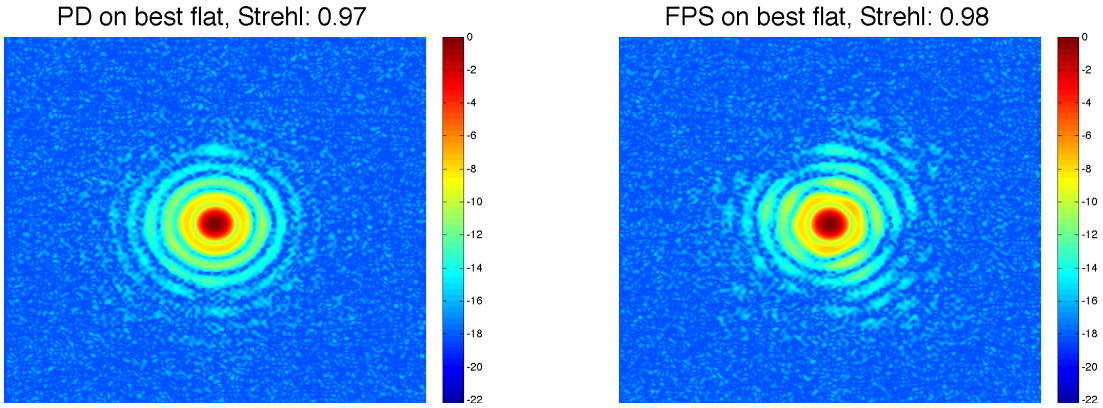

Figure 10. Correction of the NCPA error-injected PSF using Phase Diversity (left) and Focal Plane Sharpening (right); Phase Diversity appears to recover the initial phase while Focal Plane Sharpening appears to converge on a local maximum.

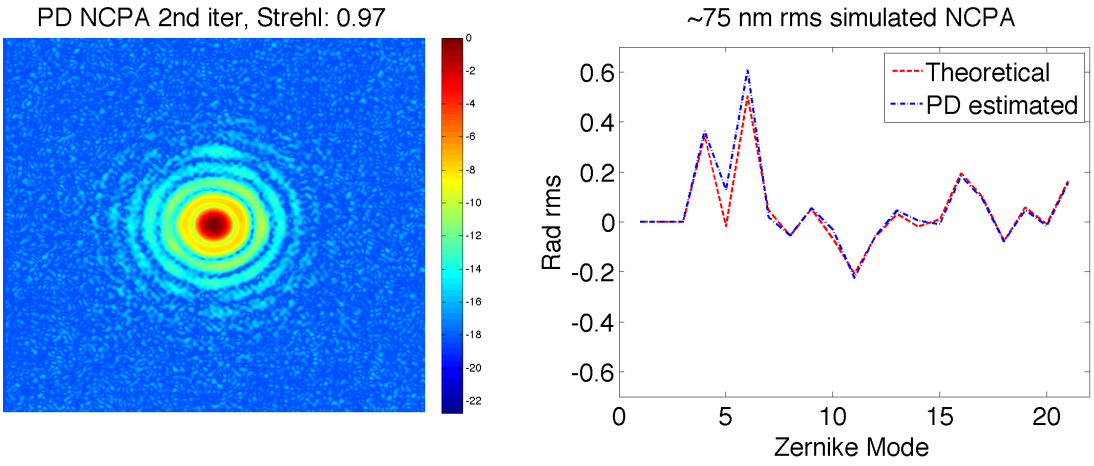

Figure 11. Left: Phase Diversity solution using the first Phase Diversity solution as a starting point, there is no obvious improvement suggesting the best solution was achieved after one iteration. Right: the first 21 Zernike modes estimated by Phase Diversity (blue) compared with the actual injected phase Zernikes (red). The Phase Diversity appears to recover the Zernikes almost perfectly.

5. THE MOAO DEMONSTRATOR RAVEN: CALIBRATION AND OBSERVATIONS

5.1 The RAVEN MOAO instrument

Typical AO applications use a 'guide star' to sample the wavefront instead of relying on the photons of the science target itself. The guide star can be an actual extra-terrestrial source or an artificial one, with the fundamental requirement it exist within the same 'region' of turbulence as the science target, defined as the 'isoplanatic angle' - typically around a few arc seconds for optical wavelengths. One issue that naturally arises from this process is the relative lack of field of view where an AO correction can be achieved; if an AO correction can be applied to

a larger field of view then this greatly broadens its astronomical applications. Contemporary AO systems aim to solve problems such as this, using techniques such as Multi-Object Adaptive Optics (MOAO), where multiple guide stars are used to define the AO-corrected field of view.

MOAO typically requires several guide stars to create an asterism on a patch of sky, within which an AO correction can be applied to one or more sub-regions. This has several astronomical applications, one such being multi-object spectroscopy where spectroscopy can benefit from the multiplexing of several AO-corrected fields. This technology has been demonstrated on the newly constructed instrument RAVEN, which was developed at the University of Victoria. RAVEN was commissioned as an MOAO demonstrator for the Subaru telescope and saw first light in May 2014. It achieved its goals by July 2015, was decommissioned, and has since been relocated to Victoria for further testing. During RAVEN's active time on Subaru, we were able to both calibrate the instrument for internal errors and then use the instrument for science observations; both are discussed here.

5.2 Calibrating the NCPA in RAVEN

In addition to using RAVEN for astronomical observations we also had the chance to test our NCPA correction methods on the instrument. Focal Plane Sharpening was successfully applied with minimal difficulty, and the resulting Strehl improvement was 30% (see Figure 12). The application of FPS was done in our earliest phase of developing the technique and thus it did not include features such as the boundary conditions discussed in Section 3.1.1. Tip/Tilt was also not estimated, which we found later to be important as it centres the PSF on a single pixel, ideal for Strehl calculations. Phase Diversity was attempted and was unsuccessful. We mainly attribute this to the fact we were not confident in the units of the applied diversity, an issue that could have been resolved if more time was permitted. Another limitation was the light source was not monochromatic but instead had a finite bandwidth, which further added complications to the code (which assumes monochromaticity). Due to the limited access to RAVEN we could not employ more tests to work through these issues; we anticipate that if we had more time we could have successfully used Phase Diversity.

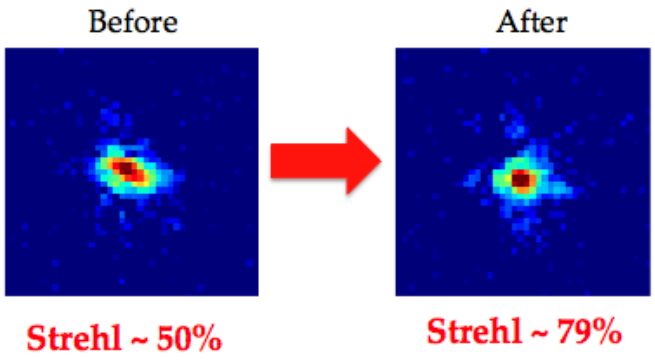

Figure 12. Focal Plane Sharpening results on RAVEN.

5.3 Early Science results with RAVEN

RAVEN feeds the Infrared Camera and Spectrograph (IRCS[13]) on the Subaru Telescope. There are other examples of systems with wide-field AO correction, such as GeMS on the Gemini South Telescope, however none have as large a field of view as RAVEN, which is up to 3.5'. This type of adaptive optics permits resolution of crowded regions (such as the Galactic Bulge or Globular Clusters) and allows for two pick-off arms to give provide simultaneous observations. Furthermore, adaptive optics operates naturally well in the infrared, a wavelength region that works extremely well with fields of high dust obscurration. Finally, if metal-poor stars in the bulge can be pre-selected, then this greatly improves the chance of finding the elusive metal-poor stars in the bulge using such an AO system.

We observed metal-poor stars in the globular cluster M22 and in the Galactic Centre using RAVEN. The scientific motivation, target selection, data reduction, and chemical abundance calculations are summarized in

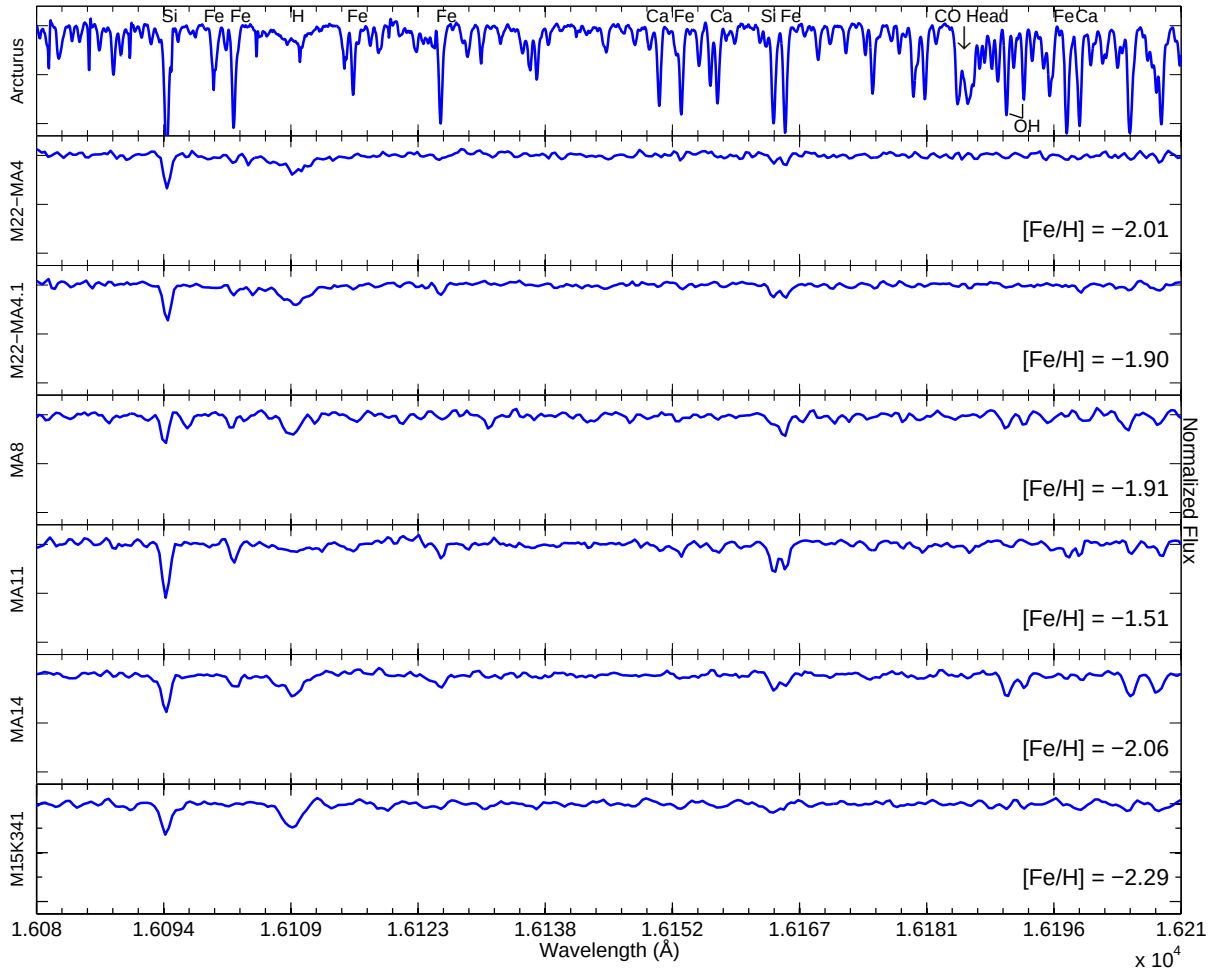

Figure 13. Sample spectral regions silicon and iron lines that were used in the abundance analysis. The higher resolution spectrum of Arcturus is also shown to highlight features in more detail.

Lamb et al. (2016, in prep.). We include here a sample of the spectra (Figure 13), which is the first high-resolution spectra ever obtain with MOAO technology and briefly discuss their scientific implications.

5.4 Scientific Implications

5.4.1 M22 stars

The GC M22 is one of the few clusters in our galaxy to have been found to show a spread in iron content (i.e. [14]) and there is current debate as to whether this spread is intrinsic or simply systematic. For example, [15] consider the iron spread can be attributed to the method in which the surface gravities are derived. They find that surface gravities that are derived spectroscopically for a sample of 17 giants yield and iron spread of ~ 0.5 dex, consistent with other works in the literature. However, when the surface gravities are derived photometrically they do not find the large intrinsic spread in iron. They find unrealistically low surface gravities when using the spectroscopic method and favour the photometric method.

The two M22 stars observed in this work were also observed by [16] at medium resolution (R$\sim$3700 and 8500), with spectroscopically derived stellar parameters; they found a metallicity difference of ~ 0.3 dex (with their RAVE pipeline). As previously mentioned, this metallicity difference was part of the motivation behind our observations. We find in this work that the iron difference between the two stars is 0.11 dex, which is on

the order of the reported error, thus showing no significant difference. In addition, the metallicities derived in this work use photometrically derived surface gravities, and so we obtain similar findings to[15] (i.e. no spread in iron). However, we only observed two targets and cannot make any statistical claim, however it is worth noting our observations are homogeneous as the stars were observed simultaneously.

5.4.2 Galactic Centre stars

The metallicity distribution function of the Galactic Centre has proven to be relative metal-rich when compared with other regions of the Galaxy, such as the halo ([17], [18]), [19])). The tail end has been shown to extend down to [Fe/H] = -3 ([20]), however there are still very few stars discovered below [Fe/H] = -1.5. Using MOAO and GLAO with RAVEN, we find 3 stars with [Fe/H] < -1.5, which are amongst some of the most metal-poor stars found in the centre of our Galaxy; their spectra are shown in Figure 13.

6. CONCLUSIONS

The conclusions we draw from this work are as follows:

- Focal Plane Sharpening outperforms Phase Diversity when starting with a system with little to no NCPA.
- Focal Plane Sharpening should be performed in closed loop in the future, or it should incorporate DM 'drift' compensations
- If typical NCPA errors are present, such as the NCPA injected here, then Phase Diversity recovers the full solution while Focal Plane Sharpening can get lost in a local maximum
- When calibrating for NCPA, Phase Diversity should always be used first, followed up with Focal Plane Sharpening (or something similar)
- Focal Plane Sharpening was easily applied to a real telescope instrument (RAVEN), where an NCPA correction resulted in a Strehl increase of 30%. Whereas Phase Diversity proved to be much more difficult, suggesting that one must understand the parameters of an AO system extremely well before attempting to use the technique.
- MOAO was used for the first time with high-resolution spectroscopy to derive chemical abundances in metal-poor stars within our Galaxy. We confirm no Fe spread in globular cluster M22 (albeit with low number statistics) and we find 3 stars in the Galactic Centre with [Fe/H] < 1.5, which are some of the most metal-poor stars observed to date.

REFERENCES

[1] van Dam, M. A., Le Mignant, D., and Macintosh, B. A., "Performance of the Keck Observatory Adaptive-Optics System," *"Applied Optics"* **43**, 5458–5467 (Oct. 2004).

[2] Roberts, Jr., L. C., Perrin, M. D., Marchis, F., Sivaramakrishnan, A., Makidon, R. B., Christou, J. C., Macintosh, B. A., Poyneer, L. A., van Dam, M. A., and Troy, M., "Is that really your Strehl ratio?," in [*Advancements in Adaptive Optics*], Bonaccini Calia, D., Ellerbroek, B. L., and Ragazzoni, R., eds., *Society of Photo-Optical Instrumentation Engineers (SPIE) Conference Series* **5490**, 504–515 (Oct. 2004).

[3] Lagarias., J., Reeds, J. A., Wright, M. H., and Wright, P. E., "Convergence Properties of the Nelder-Mead Simplex Method in Low Dimensions," *"SIAM Journal of Optimization"* **9**(1), 112–147 (1998).

[4] Lamb, M., Andersen, D. R., Véran, J.-P., Correia, C., Herriot, G., Rosensteiner, M., and Fiege, J., "Non-common path aberration corrections for current and future AO systems," in [*Society of Photo-Optical Instrumentation Engineers (SPIE) Conference Series*], *Society of Photo-Optical Instrumentation Engineers (SPIE) Conference Series* **9148**, 57 (July 2014).

[5] Dohlen, K., Wildi, F. P., Puget, P., Mouillet, D., and Beuzit, J.-L., "SPHERE: Confronting in-lab performance with system analysis predictions," in [*Second International Conference on Adaptive Optics for Extremely Large Telescopes. Online at ¡A href="http://ao4elt2.lesia.obspm.fr"¿http://ao4elt2.lesia.obspm.fr¡/A¿, id.75*], (Sept. 2011).

[6] Hartung, M., Blanc, A., Fusco, T., Lacombe, F., Mugnier, L. M., Rousset, G., and Lenzen, R., "Calibration of NAOS and CONICA static aberrations. Experimental results," *Astronomy and Astrophysics* **399**, 385–394 (Feb. 2003).

[7] Blanc, A., Fusco, T., Hartung, M., Mugnier, L. M., and Rousset, G., "Calibration of NAOS and CONICA static aberrations. Application of the phase diversity technique," *Astronomy and Astrophysics* **399**, 373–383 (Feb. 2003).

[8] Gonsalves, R. A., "Phase retrieval and diversity in adaptive optics," *Optical Engineering* **21**(5), 215829–215829– (1982).

[9] Paxman, R. G., Schulz, T. J., and Fienup, J. R., "Joint estimation of object and aberrations by using phase diversity," *Journal of the Optical Society of America A* **9**, 1027–1085 (1992).

[10] Sauvage, J.-F., Fusco, T., Rousset, G., and Petit, C., "Calibration and precompensation of noncommon path aberrations for extreme adaptive optics," *Journal of the Optical Society of America A* **24**, 2334–2346 (Aug. 2007).

[11] Paul, B., Sauvage, J.-F., and Mugnier, L. M., "Coronagraphic phase diversity: performance study and laboratory demonstration," *Astronomy and Astrophysics* **552**, A48 (Apr. 2013).

[12] Correia, C., Veran, J.-P., Guyon, O., and Clergeon, C., "Wave-front reconstruction for the non-linear curvature wave-front sensor," in [*Proceedings of the Third AO4ELT Conference*], Esposito, S. and Fini, L., eds. (Dec. 2013).

[13] Kobayashi, N., Tokunaga, A. T., Terada, H., Goto, M., Weber, M., Potter, R., Onaka, P. M., Ching, G. K., Young, T. T., Fletcher, K., Neil, D., Robertson, L., Cook, D., Imanishi, M., and Warren, D. W., "IRCS: infrared camera and spectrograph for the Subaru Telescope," in [*Optical and IR Telescope Instrumentation and Detectors*], Iye, M. and Moorwood, A. F., eds., *Society of Photo-Optical Instrumentation Engineers (SPIE) Conference Series* **4008**, 1056–1066 (Aug. 2000).

[14] Marino, A. F., Sneden, C., Kraft, R. P., Wallerstein, G., Norris, J. E., da Costa, G., Milone, A. P., Ivans, I. I., Gonzalez, G., Fulbright, J. P., Hilker, M., Piotto, G., Zoccali, M., and Stetson, P. B., "The two metallicity groups of the globular cluster M 22: a chemical perspective," *A&A* **532**, A8 (Aug. 2011).

[15] Mucciarelli, A., Lapenna, E., Massari, D., Pancino, E., Stetson, P. B., Ferraro, F. R., Lanzoni, B., and Lardo, C., "A Chemical Trompe-L'oeil: No Iron Spread in the Globular Cluster M22," *ApJ* **809**, 128 (Aug. 2015).

[16] Lane, R. R., Kiss, L. L., Lewis, G. F., Ibata, R. A., Siebert, A., Bedding, T. R., Székely, P., and Szabó, G. M., "AAOmega spectroscopy of 29 351 stars in fields centered on ten Galactic globular clusters," *A&A* **530**, A31 (June 2011).

[17] Schörck, T., Christlieb, N., Cohen, J. G., Beers, T. C., Shectman, S., Thompson, I., McWilliam, A., Bessell, M. S., Norris, J. E., Meléndez, J., Ramírez, S., Haynes, D., Cass, P., Hartley, M., Russell, K., Watson, F., Zickgraf, F.-J., Behnke, B., Fechner, C., Fuhrmeister, B., Barklem, P. S., Edvardsson, B., Frebel, A., Wisotzki, L., and Reimers, D., "The stellar content of the Hamburg/ESO survey. V. The metallicity distribution function of the Galactic halo," *A&A* **507**, 817–832 (Nov. 2009).

[18] Hill, V., Lecureur, A., Gómez, A., Zoccali, M., Schultheis, M., Babusiaux, C., Royer, F., Barbuy, B., Arenou, F., Minniti, D., and Ortolani, S., "The metallicity distribution of bulge clump giants in Baade's window," *A&A* **534**, A80 (Oct. 2011).

[19] Ness, M., Freeman, K., Athanassoula, E., Wylie-de-Boer, E., Bland-Hawthorn, J., Asplund, M., Lewis, G. F., Yong, D., Lane, R. R., and Kiss, L. L., "ARGOS - III. Stellar populations in the Galactic bulge of the Milky Way," *MNRAS* **430**, 836–857 (Apr. 2013).

[20] Howes, L. M., Asplund, M., Casey, A. R., Keller, S. C., Yong, D., Gilmore, G., Lind, K., Worley, C., Bessell, M. S., Casagrande, L., Marino, A. F., Nataf, D. M., Owen, C. I., Da Costa, G. S., Schmidt, B. P., Tisserand, P., Randich, S., Feltzing, S., Vallenari, A., Allende Prieto, C., Bensby, T., Flaccomio, E., Korn, A. J., Pancino, E., Recio-Blanco, A., Smiljanic, R., Bergemann, M., Costado, M. T., Damiani, F., Heiter, U., Hill, V., Hourihane, A., Jofré, P., Lardo, C., de Laverny, P., Magrini, L., Maiorca, E., Masseron, T., Morbidelli, L., Sacco, G. G., Minniti, D., and Zoccali, M., "The Gaia-ESO Survey: the most metal-poor stars in the Galactic bulge," *MNRAS* **445**, 4241–4246 (Dec. 2014).